

**Figure 10** Measured spectra at the receiver using Raman amplification and hybrid Raman/EDFA

and hybrid Raman/EDFA. It was demonstrated by simulation that the hybrid solution provides an equalized gain over a bandwidth of 50 nm.

An analysis of a Raman amplification solution for C + L band is also presented for normal and resilient operation. The net gain and OSNR demonstrate the feasibility of this solution for normal operation scenario but the resilient operation scenario is affected by a high gain ripple and Kerr nonlinear effects due to the high power achieved are very penalizing.

An experimental assessment of the impact of the amplification scheme on the performance of an IP 10 Gigabit Ethernet system was also accomplished, demonstrating that the hybrid scheme is more suitable for the analyzed network.

#### ACKNOWLEDGMENTS

This work was supported by the POSC program, financed by the European Union FEDER fund and by the Portuguese scientific program through projects GPON in a box. The authors also greatly acknowledge the FP7 project EUROFOS.

#### REFERENCES

1. H. Ueda, K. Okada, B. Ford, G. Mahony, S. Hornung, D. Faulkner, J. Abiven, S. Durel, R. Ballart, and J. Erickson, Deployment status and common technical specifications for a B-PON system, *IEEE Commun Mag* 39 (2001), 134–141.
2. M. McGarry, M. Maier, and M. Reisslein, Ethernet PONs: A survey of dynamic bandwidth allocation (DBA) algorithms, *IEEE Commun Mag* 42 (2004), S8–S15.
3. A. Cauvin, J. Brannan, and K. Saito, Common technical specification of the G-PON system among major worldwide access carriers, *IEEE Commun Mag* 44 (2006), 34–40.
4. C.-H. Lee, W.V. Sorin, and B.Y. Kim, Fiber to the home using a PON infrastructure, *J Lightwave Technol* 24 (2006), 4568–4583.
5. C. Bock, J. Prat, and S.D. Walker, Hybrid WDM/TDM-PON using the AWG FRS and featuring centralized light generation and dynamic bandwidth allocation, *J Lightwave Technol* 23 (2005), 3981.
6. G. Talli and P. Townsend, Hybrid DWDM-TDM long-reach PON for next generation optical access, *J Lightwave Technol* 24 (2006), 2827.
7. B. Neto, C. Reis, R.P. Dionísio, J.M. Ferreira, J.A. Lazaro, G. Tosi-Beleffi, A.N. Pinto, R. Nogueira, A. Teixeira, J. Prat, and P.S. André, Assessment and mitigation of EDFA gain transients in hybrid WDM/TDM PON in the presence of packet based traffic, *IET Optoelectron* 4 (2010), 219–226.
8. B. Neto, A. Klingler, C. Reis, R.P. Dionísio, R.N. Nogueira, A.L.J. Teixeira, and P.S. André, Enhanced optical gain clamping for

upstream packet based traffic on hybrid WDM/TDM-PON using fiber Bragg grating, *Opt Commun* 284 (2011), 1354–1356.

9. J. Lazaro, J. Prat, P. Chanclou, G. Tosi Beleffi, A. Teixeira, I. Tomkos, R. Soila, and V. Koratzinos, Scalable extended reach PON, *Opt Fiber Commun/National Fiber Optic Engineers Conference*, 2008. OFC/NFOEC 2008. February 24–28, 2008, pp. 1–3.
10. R. Davey, D. Grossman, M. Rasztovtovs-Wiech, D. Payne, D. Nesset, A. Kelly, A. Rafel, S. Appathurai, and S. Yang, Long-reach passive optical networks, *J Lightwave Technol* 27 (2009), 273–291.
11. I. Tafur Monroy, R. Kjaer, F. Ohman, K. Yvind, and P. Jeppesen, Distributed fiber Raman amplification in long reach PON bidirectional access links, *Opt Fiber Technol* 14 (2008), 41–44.
12. J.H. Lee, Y.-G. Han, S.B. Lee, and C.H. Kim, Raman amplification-based WDM-PON architecture with centralized Raman pump driven, spectrum-sliced erbium ASE and polarization-insensitive EAMs, *Opt Express* 14 (2006), 9036–9041.

© 2011 Wiley Periodicals, Inc.

## CHARACTERIZATION OF SrTiO<sub>3</sub> THIN FILMS AT MICROWAVE FREQUENCIES USING COPLANAR WAVEGUIDE LINEAR RESONATOR METHOD

J. I. Marulanda,<sup>1</sup> M. Cremona,<sup>2</sup> R. Santos,<sup>2</sup> M. C. R. Carvalho,<sup>1</sup> and L. S. Demenicis<sup>3</sup>

<sup>1</sup>Centro de Estudos em Telecomunicações da Pontifícia Universidade Católica do Rio de Janeiro (CETUC/PUC-Rio), Rio de Janeiro, RJ, Brazil; Corresponding author: jmarulan@cetuc.puc-rio.br

<sup>2</sup>Departamento de Física, Pontifícia Universidade Católica do Rio de Janeiro (PUC-Rio), Rio de Janeiro, Brazil

<sup>3</sup>Seção de Engenharia Elétrica, Instituto Militar de Engenharia, Rio de Janeiro, Brazil

Received 20 December 2010

**ABSTRACT:** Experimental characterization of the dielectric properties of a SrTiO<sub>3</sub> (STO) thin film in the microwave frequency range at room temperature is presented. The coplanar waveguide linear resonator technique, which is already well-established for thick film characterization, was tailored and improved to allow thin film measurements. Experimental results are in very good agreement with theoretical analysis. Using this approach, a relative dielectric constant of 95 and a loss tangent less than 10<sup>-3</sup> were measured for a STO film with 4.2 μm of thickness deposited by radio frequency (RF) magnetron sputtering. © 2011 Wiley Periodicals, Inc. *Microwave Opt Technol Lett* 53:2418–2422, 2011; View this article online at [wileyonlinelibrary.com](http://wileyonlinelibrary.com). DOI 10.1002/mop.26233

**Key words:** thin film characterization; high dielectric constant; strontium titanate; coplanar waveguide; microwave resonator

#### 1. INTRODUCTION

High dielectric constant films have become an important research area because of their applications in electronics and microwave industries. The use of high dielectric constant films allows the miniaturization of both active and passive components [1, 2]. Thin film capacitors, filters, resonators, and impedance transformers are some successful examples of this promising technology [3–7]. Besides miniaturization, some high dielectric constant materials, such as ferroelectric films, feature a change in dielectric permittivity as a function of an applied electric field. This property is of great interest for electrically tunable microwave devices as resonators, filters, and phase shifters [8, 9].

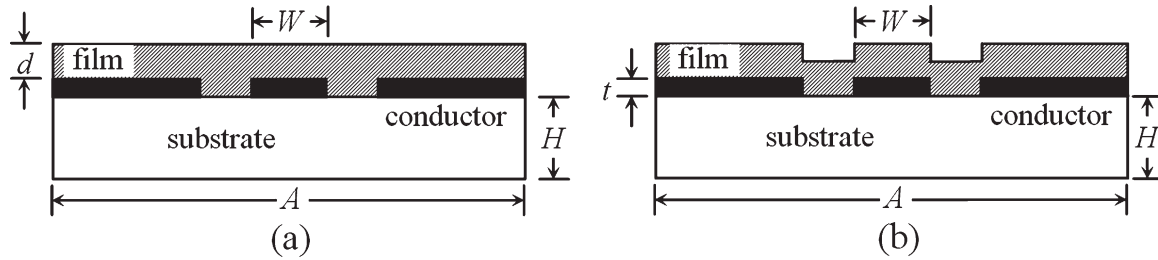


**Figure 1** Cross-sections of the resonators with film over the conductors. (a) Model used to simulate thick films deposited and (b) model for thin films

In the past two decades, materials such SrTiO<sub>3</sub> (STO), BaTiO<sub>3</sub> (BTO), and (Ba,Sr)TiO<sub>3</sub> have been intensively studied as they present a high dielectric constant in bulk form. These materials have also been investigated as ferroelectric films for their potential applications in tunable devices mentioned above.

The dielectric properties of thin films are noticeably different from those of their bulk counterparts. Specifically in the microwave frequency range these properties are very sensitive to film fabrication method, thickness, thermal treatment after film deposition, etc. Considering the STO thin film deposited by RF magnetron sputtering in particular, different values of dielectric constant and loss tangent at microwave frequencies have been reported, depending on deposition conditions [10–14]. Thus, the accurate design of high-frequency devices requires a precise characterization of film dielectric properties in this frequency range. Moreover, the parameters should be obtained in a configuration the most similar to that to be used in the final application.

Many methods have been proposed to characterize the dielectric properties of thin films. Methods including parallel plate capacitors [15], interdigital capacitors [16], phase shifters, and coplanar waveguides (CPWs) [17] have been used to extract parameters for both STO and BTO thin films. In these techniques, the film to be characterized is usually deposited on a bulk substrate and the circuit is printed over the film layer.

Recently [18], a CPW linear resonator technique for the experimental characterization of the dielectric constant and losses of thick films has been proposed and successfully used in the microwave frequency range. The approach is relatively easy to implement and consists of a film with unknown high dielectric constant deposited over the resonator printed on standard alumina substrate using conventional photolithography process. The resulting effective dielectric constant of the structure takes into account the contribution of both dielectrics and the geometry of the resonator. Comparison between experimental and theoretical results (simulations) of transmission characteristics of the resonator with frequency allows the determination of the dielectric properties of the film.

This CPW linear resonator technique was previously used to extract microwave dielectric properties at room temperature of screen printed thick films of BTO, CaCu<sub>3</sub>T<sub>4</sub>O<sub>12</sub> (CCTO), and (BTO)<sub>x</sub>-(CCTO)<sub>1-x</sub> composite with different concentrations and thickness between 100 and 120 μm at frequencies in the range of 50 MHz–20 GHz. The same technique was successfully applied to measure the dielectric constant and losses of CaTiO<sub>3</sub> (CTO), MgTiO<sub>3</sub> (MTO), and (MTO)<sub>x</sub>-(CTO)<sub>1-x</sub> composite with  $x = 0.20, 0.5$  and  $0.95$ , and 100–170 μm thickness at microwave frequencies [18, 19].

In the present work, the CPW linear resonator technique was extended and improved to allow the characterization of thin films rather than thick films. Considering the thin film case, spe-

cial attention must be done to the simulations to reproduce accurately and consistently the measured results. In this process, details on the geometry of the structures are carefully taken into account, as they are fundamental to the fidelity between model and real device. This procedure has been adopted here to determine the dielectric characteristics of a STO thin film with 4.2 μm thickness obtained by RF magnetron sputtering deposition. Dielectric constant and loss tangent obtained results are in accordance with those reported in the literature.

## 2. STRUCTURE DESCRIPTION

The CPW linear resonator configuration used in this article is depicted in Figure 1. It consists of a thin film with very high relative dielectric constant deposited over a CPW linear resonator printed on alumina substrate. The resonators are printed on Piconics® thin-film polished alumina substrate ( $\epsilon_s = 9.8$ ) with 3 μm gold metallization thickness ( $t$ ), using a conventional photolithography process. The height and width of the substrate are, respectively  $H = 635 \mu\text{m}$  and  $A = 5.0 \text{ mm}$ . The conventional cross-section of the resonators used in previous simulations of this method [18, 19] is shown in Figure 1(a). However, it cannot be applied when RF sputtered thin films are considered because the film layer follows the conductor contour. To model the real profile, caused by deposition process, a step-shaped cross-section surface has been adopted here, as shown in Figure 1(b). In this case, the relationship between film and conductor layer thicknesses must be taken into account, mainly when they are comparable in dimensions.

The thickness  $d$  of the film is measured from the top surface of the gold metallization. According to the top view of the resonator, depicted in Figure 2, the total length of the circuit is  $L = 25.4 \text{ mm}$ ; the length of the resonator middle-section is  $L_1 = 5.3 \text{ mm}$ ; the coupling gap is  $D = 150 \mu\text{m}$ ; the width of the CPW central line and lateral gap dimensions are, respectively,  $W = 450 \mu\text{m}$  and  $G = 280 \mu\text{m}$ .

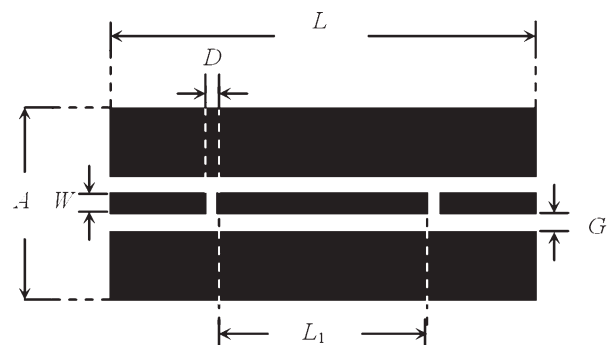


**Figure 2** Upper view of the CPW linear resonator

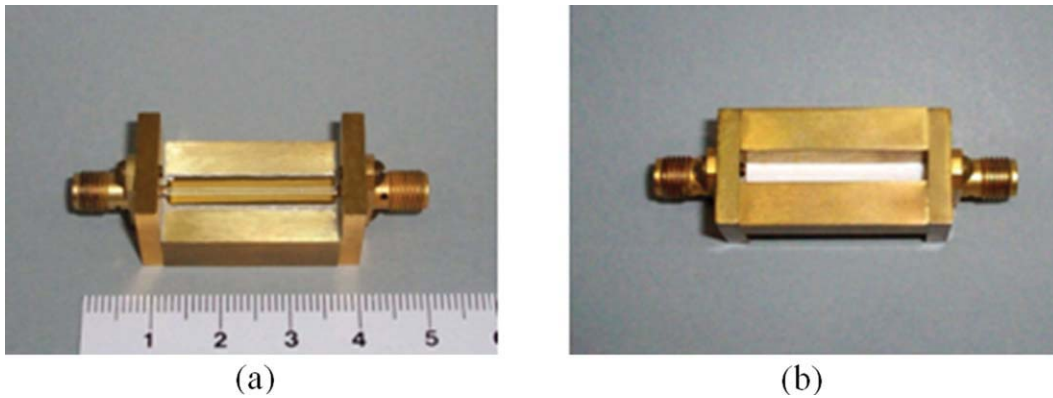


**Figure 3** (a) Top view of the assembled CPW resonator after film deposition. (b) Backside of the assembled resonator. [Color figure can be viewed in the online issue, which is available at [wileyonlinelibrary.com](http://wileyonlinelibrary.com)]

The technique is based on the resonance properties of the resonator [18, 19]. Comparison between measured results and theoretical predictions of transmission characteristics with frequency yields the determination of the dielectric properties of the film. The theoretical analysis of the resonators has been performed using a commercially available high-frequency structure simulator (Ansoft HFSS) for the electromagnetic modeling of arbitrarily shaped passive 3-D structures [20]. As all dimensions of the resonators are known, including the film thickness ( $d$ ) and shape, the dielectric constant of the film can be obtained through the frequency of the fundamental resonance peak.

### 3. EXPERIMENTAL RESULTS AND DISCUSSION

The films used in the present work were elaborated in a 450 series Leybold deposition system by RF magnetron sputtering

using a 2 inch diameter STO target with 99.9% purity (Kurt J. Lesker). The power was supplied by an RF generator (13.56 MHz) matched to the target by a tuning network, both from Advanced Energy. The STO films with a thickness of  $4.2 \mu\text{m}$  were deposited at room temperature with the following conditions: RF power of 200 W, base pressure of  $6.9 \times 10^{-7}$  Torr, work pressure of  $5.5 \times 10^{-5}$  Torr, target-substrate distance of 7.0 cm and a deposition rate of  $140 \text{ \AA}/\text{min}$ . The vacuum chamber was evacuated below  $1 \times 10^{-6}$  Torr before filling with Ar gas. No post deposition thermal treatment was performed on the films. The film thickness ( $d$ ) was measured with a Dektak 150 precision profile meter from Veeco. Photograph of the assembled resonator top view after film deposition is shown in Figure 3, where the backside was properly designed to keep the CPW configuration. Note that the reference resonator can be seen through the film because of its transparency. The lateral CPW ground planes were wire bonded to the package. Coupling to the resonator was achieved using SMA connectors.

The transmission characteristics of the resonators were measured using a HP 8720C vector network analyzer (0.05–20 GHz) at room temperature. Figure 4(a) shows the experimental insertion loss peaks obtained for the film-coated CPW resonator and the reference one (with the same physical dimensions but without film coating) in the frequency range from 50 MHz to 20 GHz. As can be seen in this figure, when the high dielectric constant film is deposited over the linear resonator, the resonance peaks of the transmission measurement are shifted to lower frequencies. This effect can be more clearly seen in Figure 4(b), where details of the fundamental resonance peaks for both resonators are shown. It is well known that the higher the dielectric constant (or the thickness of

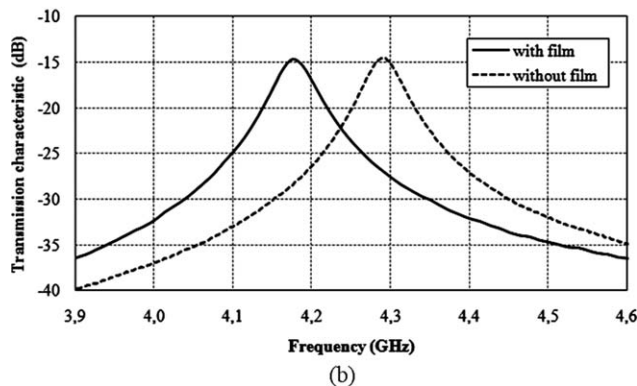
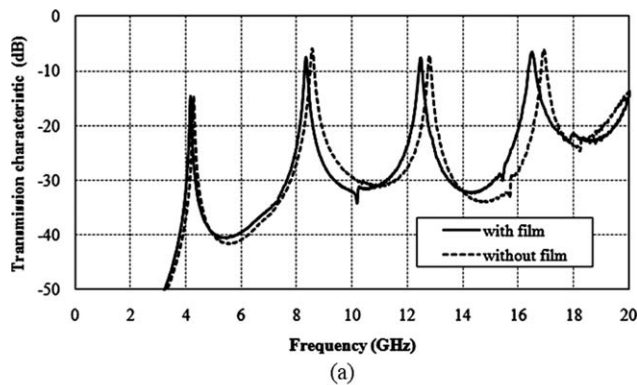


**Figure 4** (a) Measured resonance peaks of the resonators with and without film. (b) Measured fundamental resonance peaks with and without film

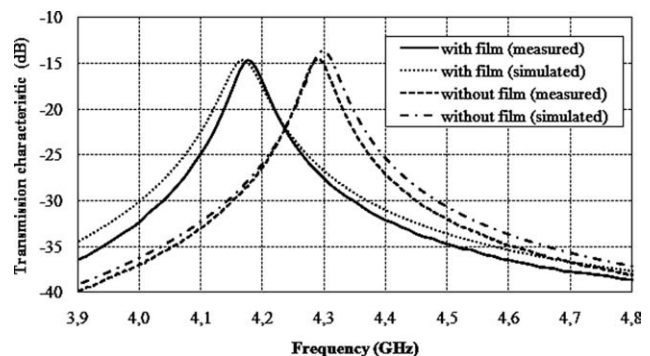


**Figure 5** Measured and simulated insertion loss for the film-coated and the reference resonators

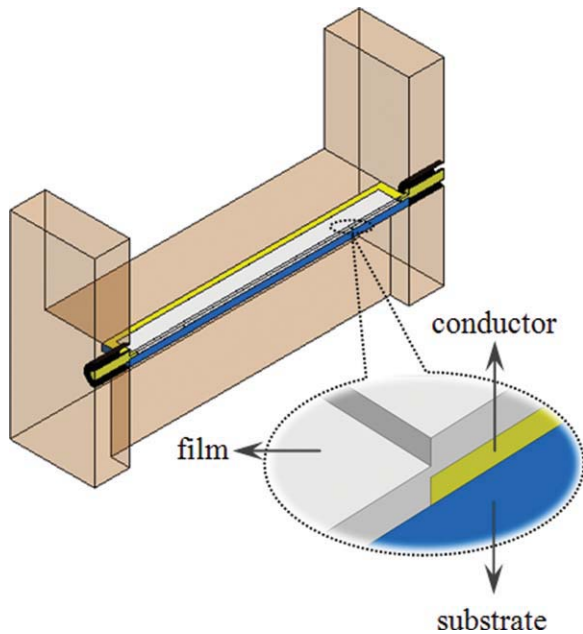


**Figure 6** Step-shaped profile of the thin film deposited over the resonator circuit. [Color figure can be viewed in the online issue, which is available at [wileyonlinelibrary.com](http://wileyonlinelibrary.com)]

the film), the higher the frequency separation between resonant peaks. Although the STO film has a high dielectric constant value, a small shift between transmission peaks was expected because of its very thin thickness. To guarantee that the observed shift was due exclusively to the dielectric film layer, careful measurements of the dimensions have been performed to assure that the fabrication process was good enough avoiding undesirable uncertainties. Measurements made with a precision profile meter (Veeco) have confirmed the step-shaped cross-section adopted by the film, as depicted in Figure 1(b).

Figure 5 shows the measured and simulated transmission curves for the film-coated and the reference resonators. It can be observed that in both cases the results are in very good agreement. From the comparison between the measured and simulated frequency response of the CPW linear resonator without film, called here as reference resonator, the relative dielectric constant and loss tangent of the alumina bulk substrate were, respectively, 9.8 and 0.0002, according to Piconics specifications.

The same procedure was used to obtain the relative dielectric constant value for the STO thin film as 95 and a very small loss tangent (less than  $10^{-3}$ ). These results are in agreement with those presented in the literature, where values between 20 and 500 have been reported for STO thin films, depending on the deposition technique, sample doping, annealing, etc [10–14].

In the adjustment process between theoretical and measured results, several simulations were performed using different dielectric parameters. The adopted shape of the thin film after the deposition over the resonator circuit, illustrated in the longitudinal cut section of the simulated structure in Figure 6, was fundamental in this process. Otherwise, underestimated values for the dielectric constant could be obtained.

It is worthy to mention that it is possible to establish a relationship between the fundamental resonance frequency and dielectric constant of the film, as performed in [18, 19]. Several CPW linear resonators can be designed and analyzed theoretically considering different thickness films for a given CPW linear resonator geometry. From these sets of curves it could be

possible to estimate the film relative dielectric constant in a simple and straightforward way, as done in [18, 19].

#### 4. CONCLUSIONS

Dielectric constant and losses of a STO RF sputtered thin film were measured for the first time in the microwave frequency range at room temperature using the CPW linear resonator method extended for thin film characterization. Experimental results are in very good agreement with theoretical analysis. The dielectric constant value measured was 95 and the loss tangent was found to be less than  $10^{-3}$  for the STO film of 4.2  $\mu\text{m}$  of thickness.

#### ACKNOWLEDGMENTS

The STO films were fabricated at Thin Films Laboratory, Department of Physics, PUC-Rio, Brazil. The resonators were printed by photolithography at LabSem (Semiconductor Laboratory), PUC-Rio, Brazil. All microwave measurements were carried out at CETUC/PUC-Rio, Brazil.

#### REFERENCES

1. M. Tanabe, M. Nishitsuji, Y. Anda, and Y. Ota, A low-impedance coplanar waveguide using an SrTiO<sub>3</sub> thin film for GaAs power MMIC's, *IEEE Trans Microwave Theory Tech* 48 (2000), 872–874.
2. F.W. Van Keuls, R.R. Romanofsky, and F.A. Miranda, Several microstrip-based conductor/thin film ferroelectric phase shifter designs using (YBa<sub>2</sub>Cu<sub>3</sub>O<sub>7- $\delta$</sub> , Au)/SrTiO<sub>3</sub>/LaAlO<sub>3</sub> structures, 10th International Symposium on Integrated Ferroelectrics, Monterey, California (1998).
3. A. Tombak, J.P. Maria, F.T. Ayguavives, Z. Jin, G.T. Stauff, A.I. Kingon, and A. Mortazawi, Voltage-controlled RF filters employing thin-film barium–strontium–titanate tunable capacitors, *IEEE Trans Microwave Theory Tech* 51 (2003), 462–467.
4. C. Weil, P. Wrang, H. Downar, J. Wenger, and R. Jakoby, Tunable coplanar waveguide phase shifters using ferroelectric thick films, *Institut fur Hochfrequenztechnik-TUD* (2002), 83–88.
5. N. Fukushima, K. Abe, M. Izuha, T. Schimizu, and T. Kawakubo, Epitaxial (Ba,Sr)TiO<sub>3</sub> capacitors with extremely high dielectric constant for DRAM applications, *IEEE-IEDM 97* (1997), 257–260.
6. A.T. Findikoglu, Q.X. Jia, I.H. Campbell, X.D. Wu, D. Reagor, C.B. Mombourquette, and D. McMurry, Electrically tunable coplanar transmission line resonators using YBa<sub>2</sub>Cu<sub>3</sub>O<sub>7- $\delta$</sub> /SrTiO<sub>3</sub> bilayers, *Appl Phys Lett* 66 (1995), 3674–3676.
7. D. Kuylenstierna, G. Subramanyam, A. Vorobiev, and S. Gevorgian, Tunable electromagnetic bandgap performance of CPW periodically loaded by ferroelectric varactors, *Microwave Opt Technol Lett* 39 (2003), 81–86.
8. A.K. Tagantsev, V.O. Sherman, K.F. Astafiev, J. Venkatesh, and N. Setter, Ferroelectric materials for microwave tunable applications, *J Electroceram* 11 (2003), 5–66.
9. O.G. Vendik, Ferroelectric films in microwave technique: Physics, characterization and tunable devices, *MSMW'04 Symposium Proceedings*, Kharkov, Ukraine, June 21–26, 2004, pp 66–71.
10. T.R. Taylor, P.J. Hansen, N. Pervez, B. Acikel, R.A. York, and J.S. Speck, Influence of stoichiometry on the dielectric properties of sputtered strontium titanate thin films, *J Appl Phys* 94 (2003), 3390–3396.
11. K. Radhakrishnan, C.L. Tan, H.Q. Zheng, and G.I. Ng, Preparation and characterization of RF-sputtered SrTiO<sub>3</sub> thin films, *J Vac Sci Technol A* 18 (2000), 1638–1641.
12. K. Akedo, H. Fujikawa, M. Suzuki, and Y. Taga, Highly insulated SrTiO<sub>3</sub> thin films, *Ion Implantation Technology Proceedings, 1998 International Conference*, 2, 1998, pp 970–973.
13. S.H. Nam and H.G. Kim, The effect of heat treatment on the SrTiO<sub>3</sub> thin films prepared by radio frequency magnetron sputtering, *J Appl Phys* 72 (1992), 2895–2899.
14. W.B. Pennebaker, RF sputtered strontium titanate films, *IBM J Res Develop*, 1969, 686–695.
15. C. Gupta, A new microwave method of measuring complex dielectric constant of high-permittivity thin films, *IEEE Trans Instrum Meas* IM-24 (1975), 61–65.

16. S.H. Nam, N.H. Cho, and H.G. Kim, Characterization of SrTiO<sub>3</sub> thin films prepared by RF magnetron sputtering, *J Phys D: Appl Phys* 25 (1992), 727–729.
17. P.K. Petrov, E.F. Carlsson, P. Larsson, M. Friesel, and Z.G. Ivanov, Improved SrTiO<sub>3</sub> multilayers for microwave application: Growth and properties, *J Appl Phys* 84 (1998), 3134–3140.
18. L.S. Demenicis, R.A.A. Lima, L.F.M. Conrado, W. Margulis, and M.C.R. Carvalho, A CPW linear resonator method for the microwave characterization of high dielectric constant films, *Microwave Opt Technol Lett* 49 (2007), 521–524.
19. J.I. Marulanda, R.A.A. Lima, M.C.R. Carvalho, A.F.L. Almeida, A.B.S. Sombra, and L.S. Demenicis, Characterization of dielectric properties of screen-printed MgTiO<sub>3</sub>–CaTiO<sub>3</sub> composite thick films in the microwave frequency range, 2009 SBMO/IEEE MTT-S International Microwave & Optoelectronics Conference (IMOC 2009), Belem, Brazil, 2009, pp 211–214.
20. Ansoft HFSS V12 user's guide, Pittsburgh, PA, 2010.

© 2011 Wiley Periodicals, Inc.

## EFFECT OF AIR-GAP ON AXIAL RATIO OF LOW PROFILE SPIRAL ANTENNA

Ali M. Mehrabani and Lotfollah Shafai

Department of Electrical and Computer Engineering, University of Manitoba, EITC, Winnipeg, Manitoba, Canada R3T 5V6; Corresponding author: shafai@ee.umanitoba.ca

Received 20 December 2010

**ABSTRACT:** A low-profile offset-fed spiral antenna over an artificial magnetic conductors (AMC) ground plane is studied in which the AMC ground plane has a two-layer structure with an air-gap present between the layers. The effect of such air gaps on the axial ratios of the antenna is investigated. The predicted numerical results are verified by testing a prototype sample of the proposed antenna showing a satisfactory agreement between them. © 2011 Wiley Periodicals, Inc. *Microwave Opt Technol Lett* 53:2422–2423, 2011; View this article online at [wileyonlinelibrary.com](http://wileyonlinelibrary.com). DOI 10.1002/mop.26248

**Key words:** spiral antenna; low profile antenna; circular polarization

### 1. INTRODUCTION

Among planar antennas, a single turn Archimedean spiral antenna [1] is an excellent candidate for circular polarization applications. With a traditional perfect electric conductor (PEC), as a ground plane, the overall height of quarter wavelength is at least required. To develop a low-profile structure, artificial magnetic conductors (AMC) are interesting alternatives to the reflecting ground surface in antenna applications. In [2–4], considerable efforts have been focused on decreasing the overall height of the antennas. Among which, a very compact and low-profile spiral antenna was designed and fabricated with a distance of only  $0.02\lambda_0$  in [4], where  $\lambda_0$  is the free-space wavelength at 4.5 GHz. To support the antenna in such a close proximity to the AMC ground plane, the antenna is etched on a dielectric substrate. The resulting air-gap between the layers due to the fabrication process will have an inevitable impact on the antenna performance. The effect of this air gap will be studied in this letter. It will be shown that the frequency behavior of the antenna can be controlled by different sizes of the air gap.

### 2. GEOMETRY OF THE PROBLEM

Conventionally, a planar spiral antenna consists of three parts: a single turn Archimedean spiral, radial linear, and the vertical feed probe. The last two parts are used to feed the antenna and

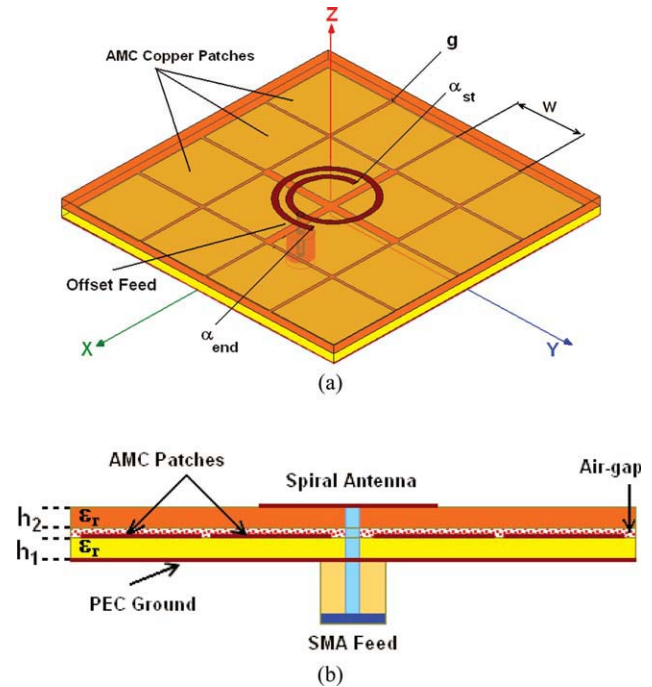


**Figure 1** (a) Top view (b) cross-section view of the offset fed curl antenna over the AMC ground plane,  $\alpha_{st} = 5\pi$ ,  $a = 0.3375$  mm/rad,  $n = 1.57253$  turns,  $\epsilon_r = 2.5$ , and  $D_{edge} = 1.55$  mm, with feed located at  $x = 6.36$  mm and  $y = 0$ ,  $h_1 = h_2 = 1.5748$  mm. [Color figure can be viewed in the online issue, which is available at [wileyonlinelibrary.com](http://wileyonlinelibrary.com)]

their contributions to the radiation pattern are very small and negligible. As a result, the radial linear section is removed, and the antenna is fed directly at the spiral part resulting in an offset-fed spiral antenna as shown in Figure 1, with an inward spiral extension as a tuning stub. The equation of Archimedean spiral curve in polar coordinates is given by  $r = a\alpha + r_0$ , where  $r_0$  and  $r$  are the radial distances from the origin at the angles (in radians)  $\alpha_{st}$  and  $\alpha$ , respectively, and  $a$  (mm/rad) is the spiral constant representing the flare rate of the spiral.

The AMC structure used in the proposed antenna is the same as reported in [4], which is an array of  $4 \times 4$ -square patches

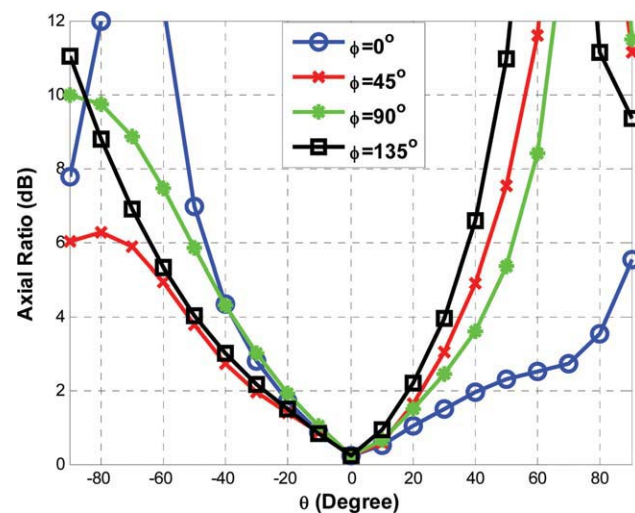


**Figure 2** Axial ratio of the antenna shown in Figure 1, when  $n = 1.57253$  turns,  $a = 0.3375$  mm/rad,  $D_{edge} = 1.55$  mm,  $\epsilon_r = 2.5$ , and  $f = 4.5$  GHz at  $\phi = 0^\circ, 45^\circ, 90^\circ$ , and  $135^\circ$  planes,  $h_1 = h_2 = 1.5748$  mm. [Color figure can be viewed in the online issue, which is available at [wileyonlinelibrary.com](http://wileyonlinelibrary.com)]